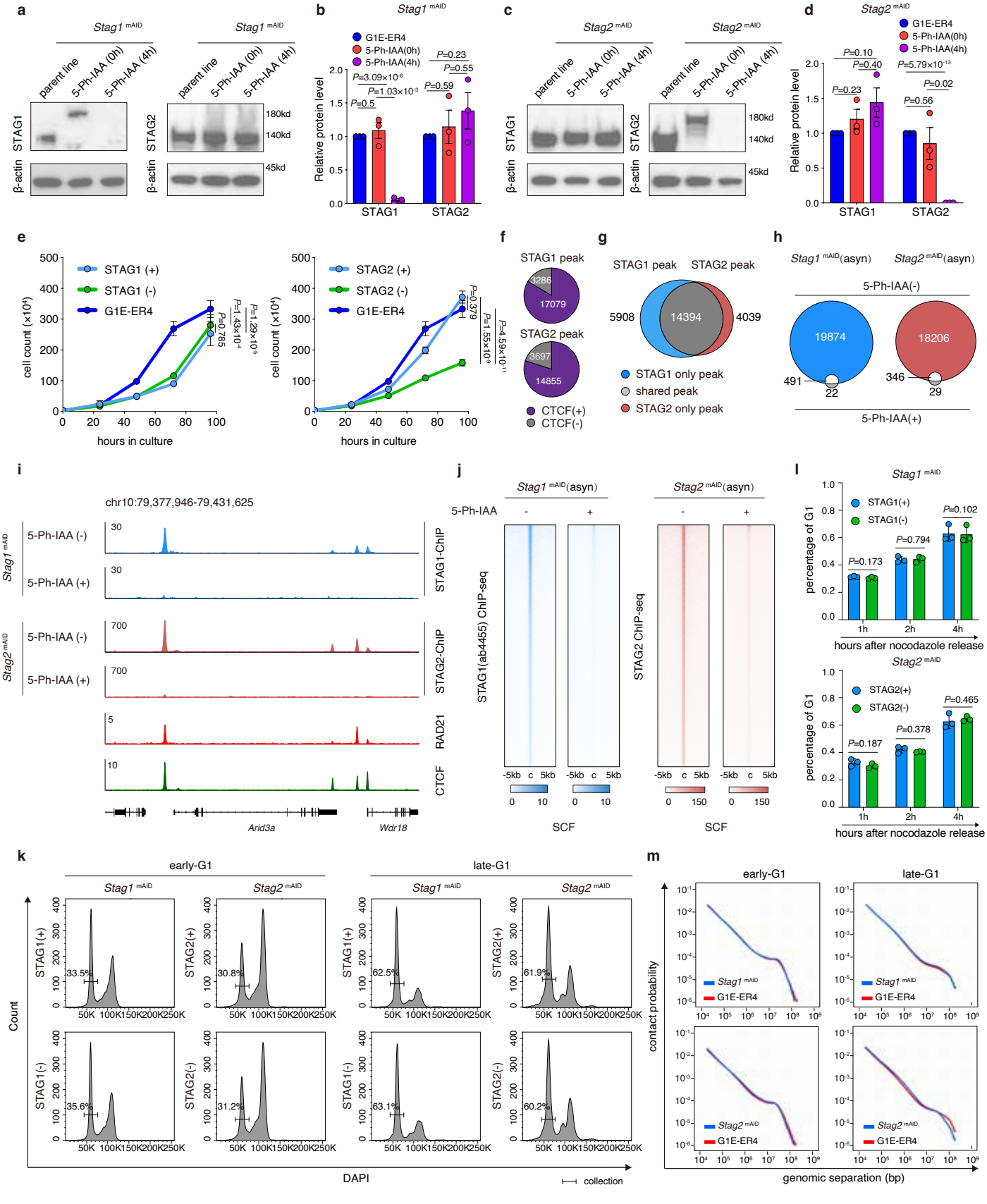
Supplementary Figure 1

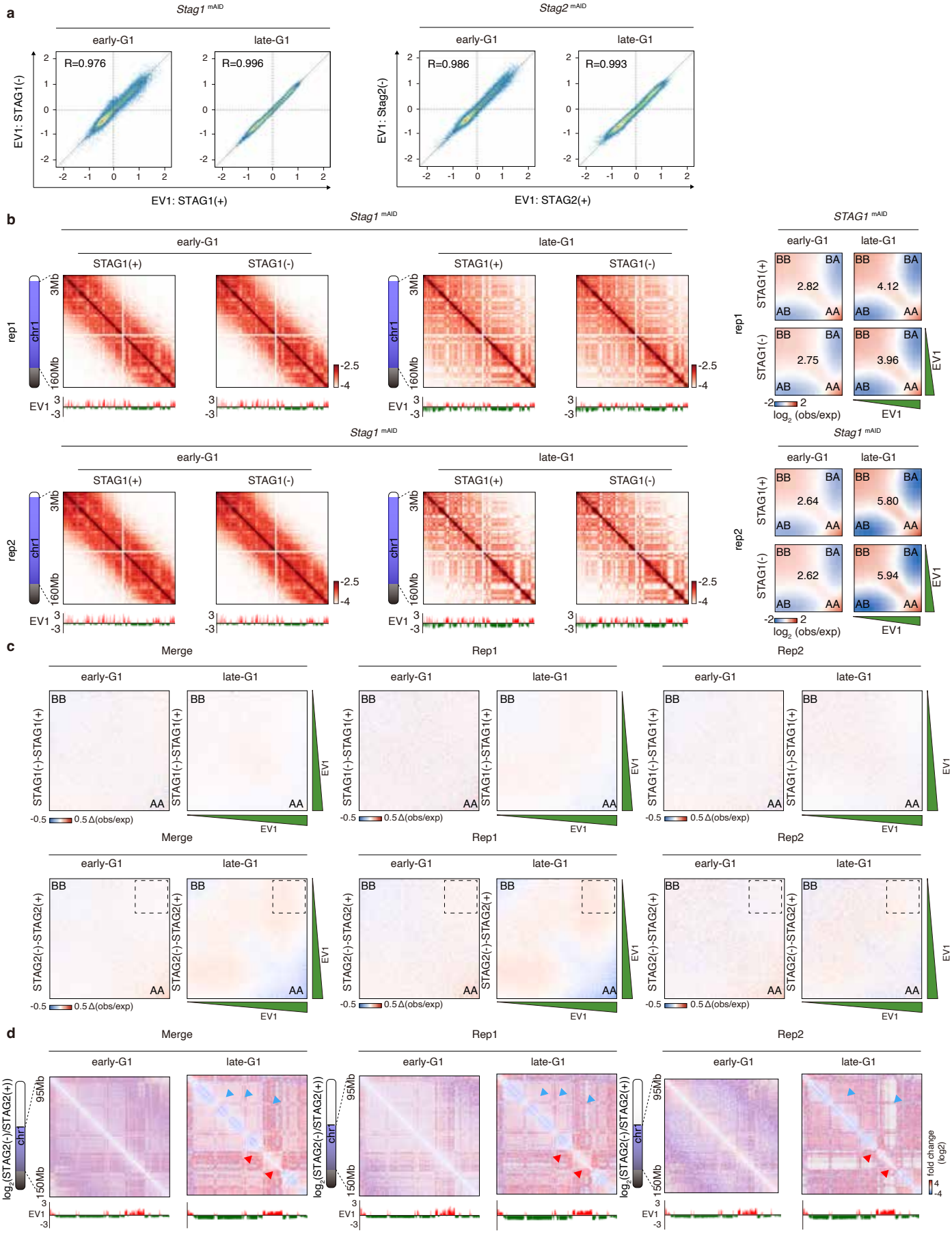


Supplementary Figure. 1: Characterization of *Stag1*^{mAID} and *Stag2*^{mAID} cell lines.

a, Immunoblot analysis of endogenous STAG1 and STAG2 protein levels in *Stag1*^{mAID} cells with or without 5-Ph-IAA treatment. STAG1 was efficiently depleted upon auxin treatment, whereas STAG2 protein abundance was unaffected. **b,** Quantification of (a). Signals were normalized to β-actin and expressed relative to parental G1E-ER4 cells, which were set to 1. Bars indicate mean and error bars indicate s.e.m.; $n = 3$. *P* values were calculated using two-sided Student's *t*-tests. **c-d,** Same as (a-b), but for *Stag2*^{mAID} cells, showing efficient depletion of STAG2 with no detectable change in STAG1 protein level. **e,** Growth curves of *Stag1*^{mAID} and *Stag2*^{mAID} cells with or without target protein depletion, shown together with the unedited parental G1E-ER4 cells. Data are mean ± s.e.m. from three independent biological replicates. *P* values were calculated using two-way repeated-measures ANOVA with Tukey's multiple-comparisons test. **f,** Pie charts showing the overlap of STAG1 and STAG2 ChIP-seq peaks with CTCF peaks. **g,** Venn diagram comparing STAG1 and STAG2 peak locations. Peaks were considered shared if their genomic coordinates overlapped. To avoid redundant counting, overlapping peaks from the two datasets were merged into non-redundant loci before quantification. **h,** Venn diagrams showing the numbers of STAG1 and STAG2 peaks in asynchronous cells before and after 5-Ph-IAA treatment. **i,** Representative genome browser tracks showing loss of STAG1 or STAG2 ChIP-seq signal upon 5-Ph-IAA treatment in *Stag1*^{mAID} and *Stag2*^{mAID} cells, respectively. RAD21 and CTCF ChIP-seq tracks for the same region are shown below. **j,** Heat maps of SCF-normalized STAG1 or STAG2 ChIP-seq signals centered at peak summits (±5 kb) in asynchronous *Stag1*^{mAID} and *Stag2*^{mAID} cells with or without 5-Ph-IAA treatment, showing efficient removal of chromatin-bound STAG1 or STAG2 after auxin treatment. **k,** Representative flow-cytometry profiles of DNA content after nocodazole release. **l,** Bar graphs showing the percentage of G1-phase cells at the indicated time points after nocodazole release in *Stag1*^{mAID} and *Stag2*^{mAID} cells with or without 5-Ph-IAA treatment. These results indicate that short-term cell-cycle progression after mitotic release is not

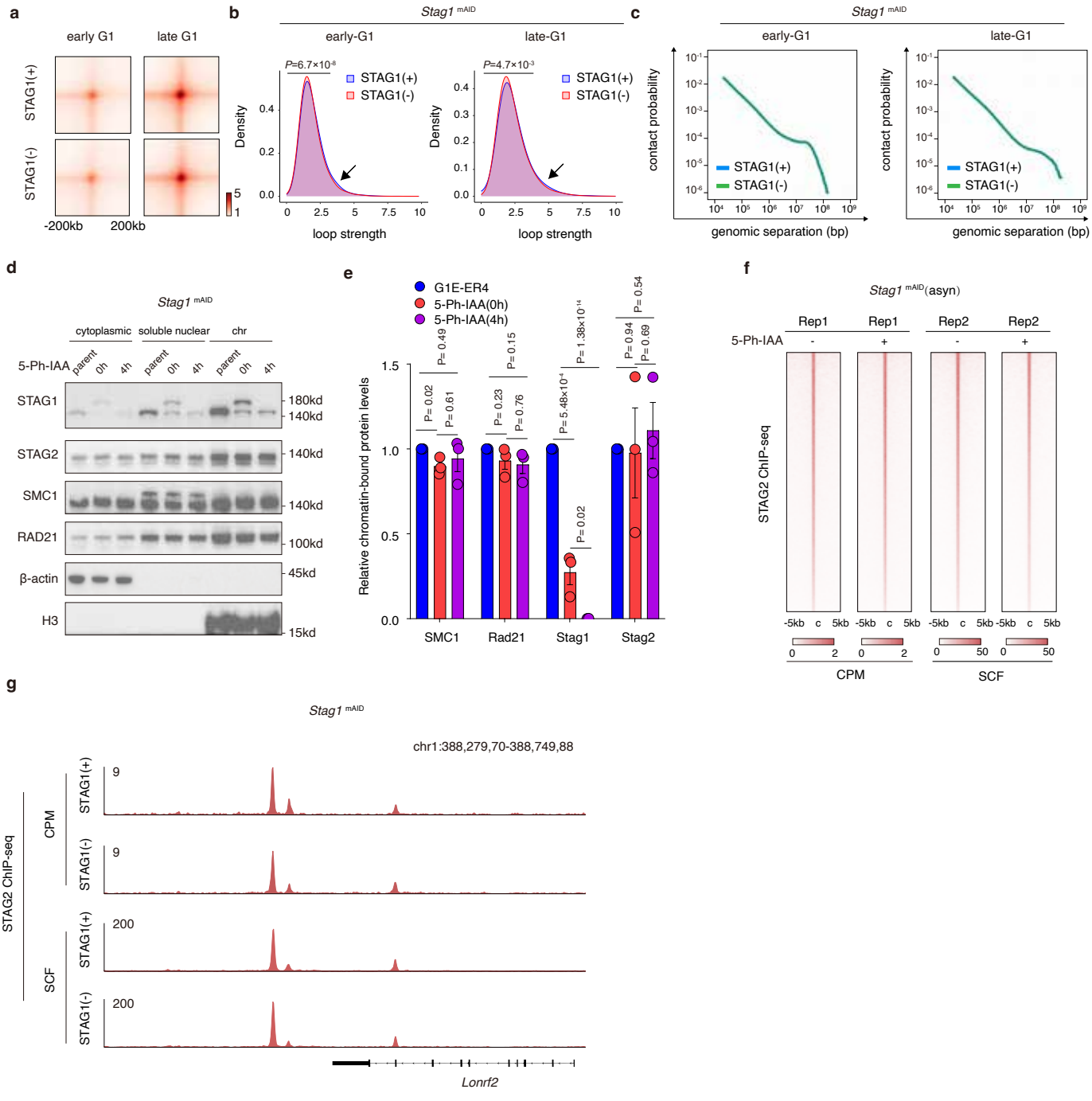
detectably altered by STAG1 or STAG2 depletion. Data are mean ± s.d. from three biological replicates. *P* values were calculated using two-tailed Student's *t*-tests. **m,** P_S curves for early-G1 and late-G1 *Stag1*^{mAID} and *Stag2*^{mAID} cells compared with the parental G1E-ER4 cells, showing that endogenous tagging does not measurably affect chromosome contact scaling and that loop extrusion remains comparable to the parental line. Source data are provided as a Source Data file.

Supplementary Figure 2



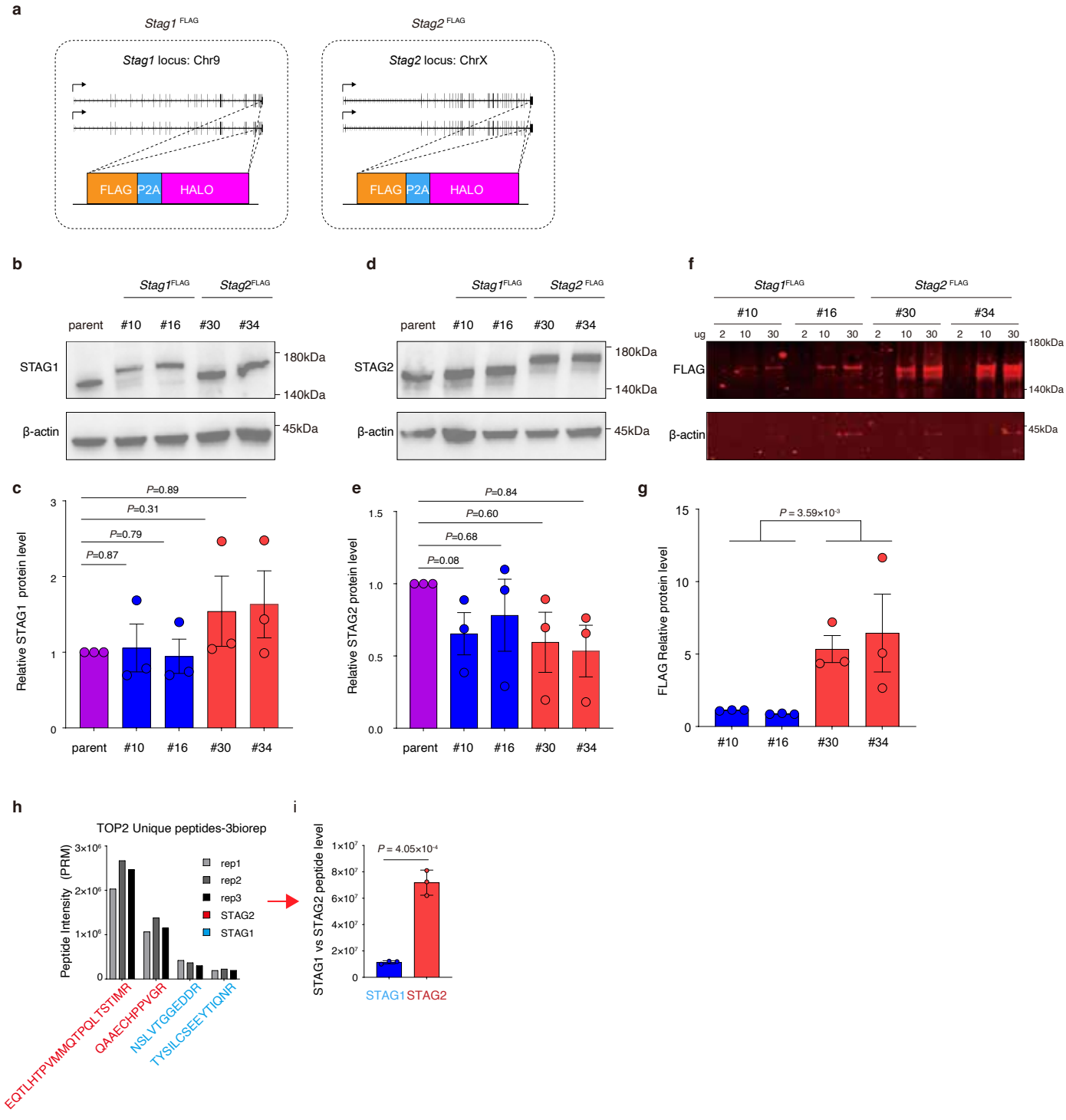
Supplementary Figure. 2: Hi-C reproducibility and compartment analysis in STAG1 or STAG2 depleted cells after mitosis. a, Scatter plots showing highly correlated EV1 values between STAG1- or STAG2-replete and -depleted samples in early-G1 and late-G1 phases. **b**, Representative KR-balanced, 100 kb-binned Hi-C contact maps from two individual biological replicates showing post-mitotic compartment reformation in *Stag1*^{mAID} cells with or without STAG1 depletion. Corresponding EV1 tracks are shown below each contact map. Saddle plots for each replicate are shown on the right. **c**, Subtracted saddle plots comparing STAG1 or STAG2 depleted samples with their corresponding replete controls. STAG1 depletion causes minimal changes in compartmentalization in both early and late-G1, whereas STAG2 depletion slightly reduces A/B compartment segregation specifically in late-G1. Results for merged samples and individual biological replicates are shown. **d**, Representative differential Hi-C contact maps showing changes in chromatin compartmentalization upon STAG2 loss in early-G1 and late-G1 phases. Gain of B–B compartment interactions and loss of A–B segregation are indicated by blue and red arrows, respectively. Results for replicate-merged and individual biological replicate samples are shown. Source data are provided as a Source Data file.

Supplementary Figure 3



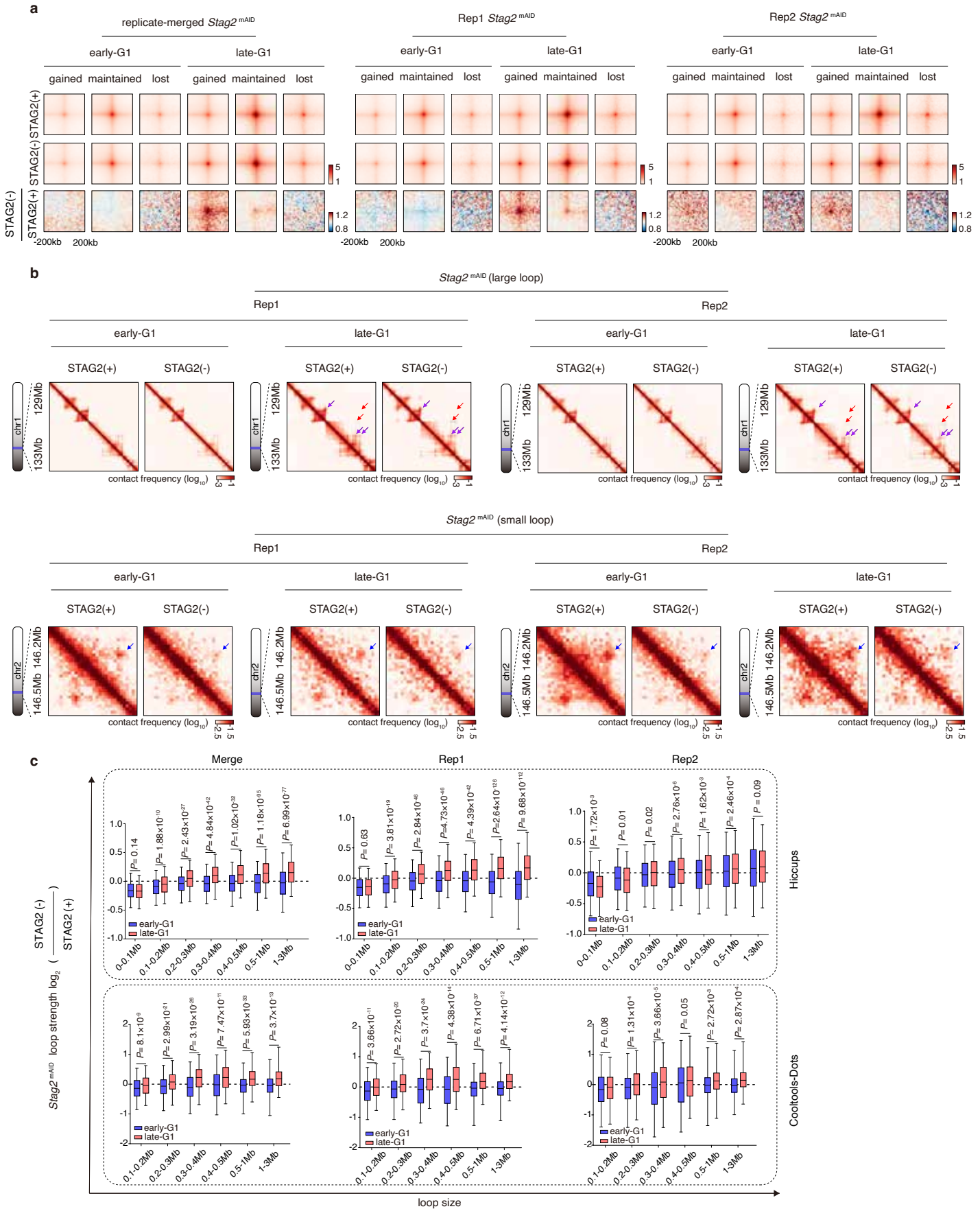
Supplementary Fig. 3: Minimal effects of STAG1 depletion on post-mitotic loop architecture and STAG2 chromatin occupancy. a, APA plots of structural loops in early-G1 and late-G1 *Stag1*^{mAID} cells with or without STAG1 depletion, showing no obvious change in loop enrichment upon STAG1 loss. **b,** Density plots of structural loop strength in early-G1 and late-G1 *Stag1*^{mAID} cells with or without STAG1 depletion. For STAG1(+) and STAG1(−) cells, n = 9,425 and 9,426 loops in early G1, respectively, and n = 9,420 loops for both groups in late G1. Arrows indicate a very slight reduction in loop strength upon STAG1 loss. *P* values were calculated using two-sided Wilcoxon rank-sum tests. **c,** P_S curves for early-G1 and late-G1 *Stag1*^{mAID} cells with or without STAG1 depletion, showing that contact scaling is largely unchanged upon STAG1 loss. **d,** Representative immunoblots from chromatin fractionation experiments in *Stag1*^{mAID} cells showing efficient removal of STAG1 from the chromatin fraction upon 5-Ph-IAA treatment, whereas chromatin-associated STAG2, SMC1, and RAD21 remain largely unchanged (cytoplasmic, cytoplasmic fraction; soluble nuclear, soluble nuclear fraction; chr, chromatin fraction). **e,** Quantification of d, Signals were normalized to H3 and expressed relative to parental G1E-ER4 cells, which were set to 1. Bars indicate mean and error bars indicate s.e.m.; dots represent independent experiments; $n = 3$. *P* values were calculated using two-sided Student's *t*-tests. **f,** Heat maps of STAG2 ChIP-seq signals in asynchronous *Stag1*^{mAID} cells with or without 5-Ph-IAA treatment, shown using both SCF and CPM normalization. Results from two biological replicates are shown and indicate that STAG2 chromatin occupancy is not detectably altered upon STAG1 depletion. **g,** Representative genome browser tracks of STAG2 ChIP-seq signals in asynchronous *Stag1*^{mAID} cells with or without 5-Ph-IAA treatment, displayed using both SCF and CPM normalization, showing no obvious change in STAG2 occupancy upon STAG1 loss. All Hi-C analyses in this figure were performed using replicate-merged Hi-C data from two biological replicates. Source data are provided as a Source Data file.

Supplementary Figure 4



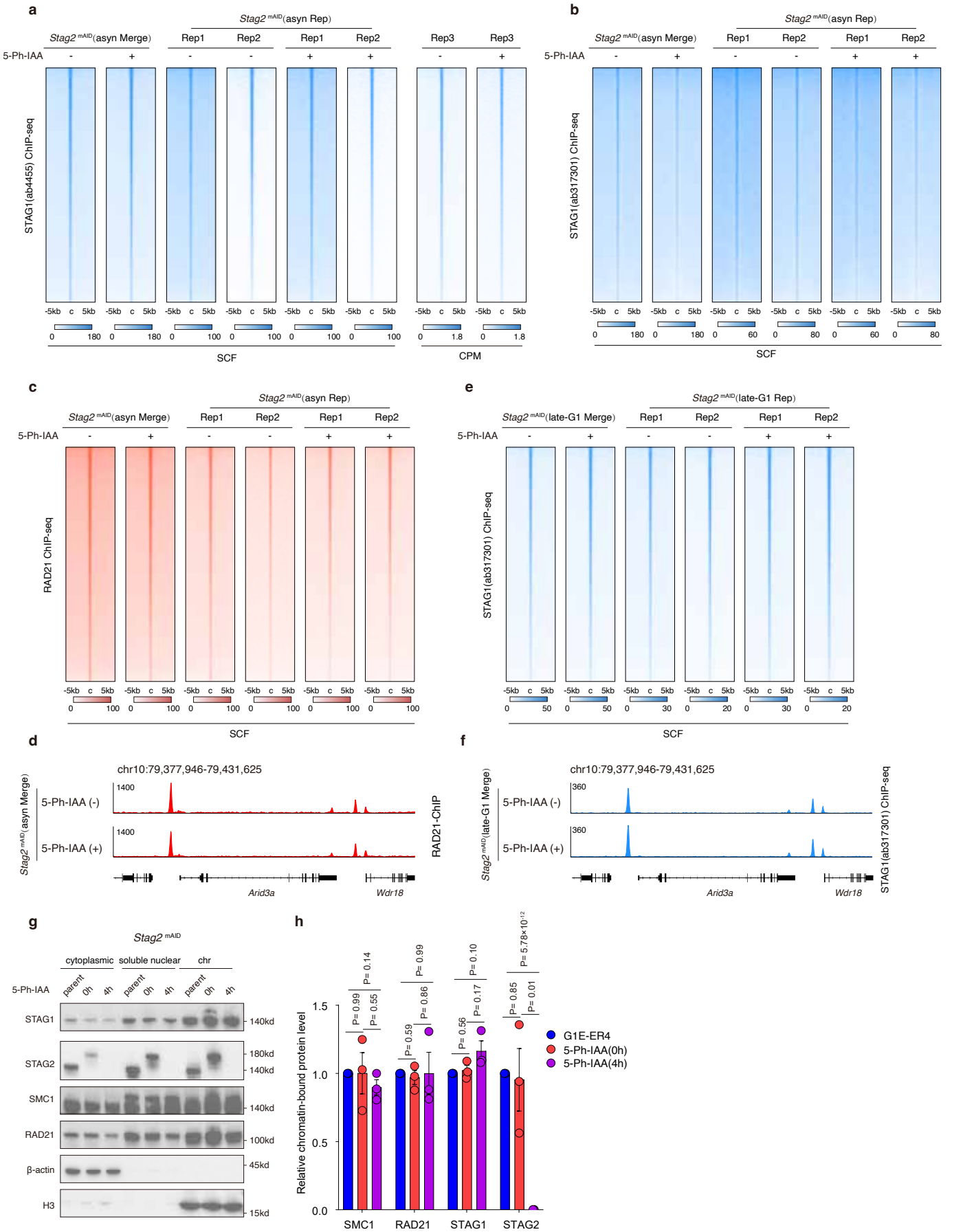
Supplementary Fig. 4: Quantification of STAG1 and STAG2 level. a, Schematic illustration of the *Stag1*^{FLAG} and *Stag2*^{FLAG} knock-in strategies. **b,** Immunoblot analysis of endogenous STAG1 protein in parental cells, two independent *Stag1*^{FLAG} clones and two independent *Stag2*^{FLAG} clones, showing that FLAG-P2A-HALO tagging does not obviously alter STAG1 protein abundance relative to the parental cells. Three independent biological replicates were performed. **c,** Quantification of (**b**). STAG1 signals were normalized to β-actin and expressed relative to parental G1E-ER4 cells, which were set to 1. Bars indicate mean and error bars indicate s.e.m.; dots represent independent experiments; $n = 3$. *P* values were calculated using two-sided Student's *t*-tests. **d-e,** Same as (b, c), but for endogenous STAG2 protein. **f,** Fluorescent immunoblot detection of FLAG signal using graded amounts of total protein lysate from the indicated clones. Three independent biological replicates were performed. **g,** Quantification of FLAG signals in (**f**). FLAG signals were normalized to β-actin and then normalized within each replicate to the mean of the two *Stag1*^{FLAG} clones (#10 and #16). Individual clone values are shown separately. The indicated *P* value was calculated by comparing pooled normalized values from the two *Stag1*^{FLAG} clones (#10 and #16; n = 6) with those from the two *Stag2*^{FLAG} clones (#30 and #34; n = 6) using a two-sided unpaired Student's *t*-test. Bars indicate mean and error bars indicate s.e.m.; dots represent independent experiments. **h,** Mass spectrometry-based quantification of the top two unique peptides for STAG1 and STAG2 across three biological replicates. **i,** Summed peptide intensities of the top two unique peptides shown in (**h**), Bars indicate mean and error bars indicate s.d.; dots represent independent biological replicates; n=3. *P* value was calculated using a two-sided unpaired Student's t-test. The result indicates an approximate STAG2:STAG1 protein abundance ratio of 5:1. Source data are provided as a Source Data file.

Supplementary Figure 5



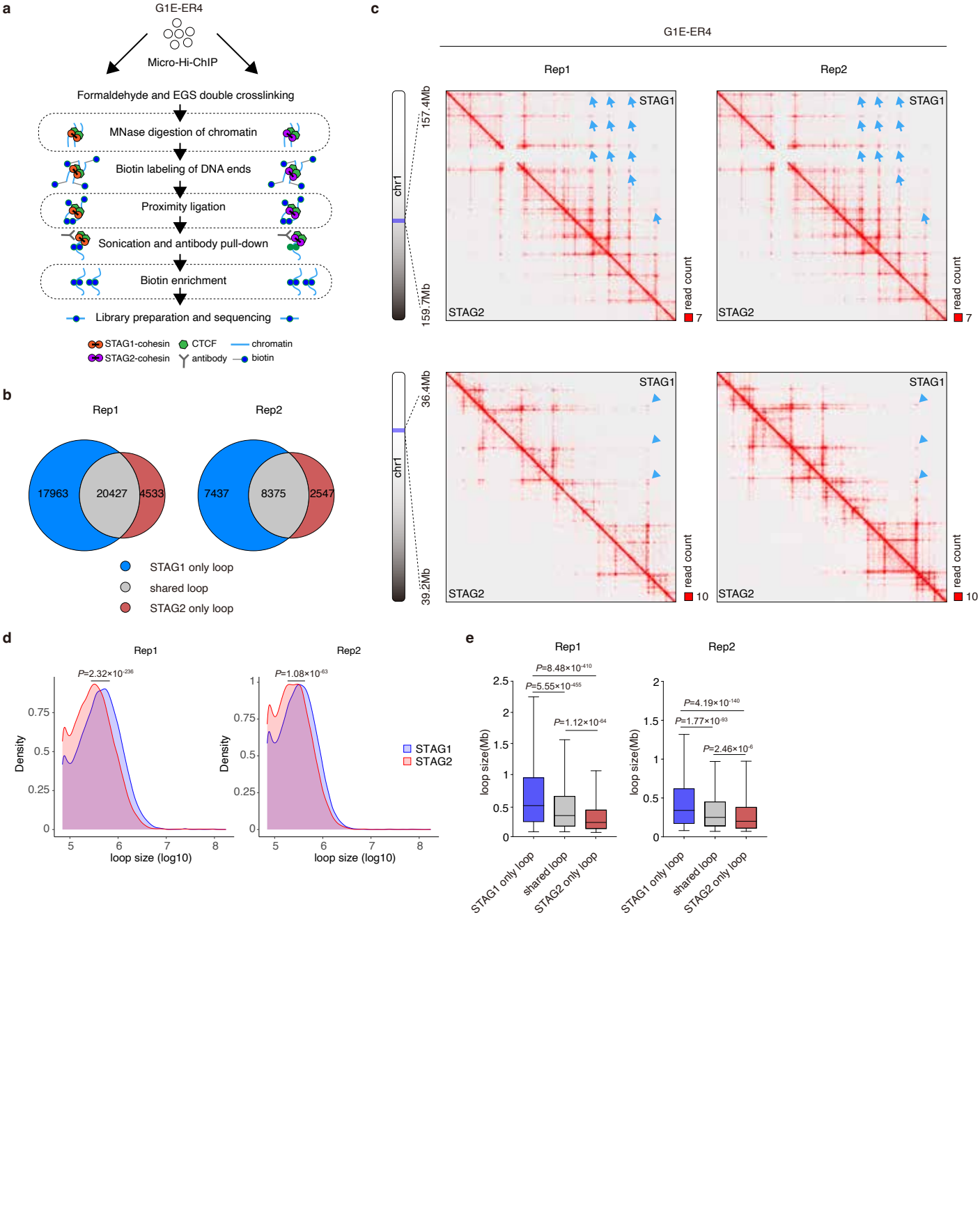
Supplementary Fig. 5: STAG2 depletion affects post-mitotic structural loop reformation. a, APA plots showing the changes of lost, maintained and gained loops upon STAG2 depletion in early- and late-G1 phase cells. Results of replicate-merged and individual replicates are shown. **b**, Hi-C contact maps showing representative gained and lost loops upon STAG2 depletion in early- and late-G1 phase. lost, maintained and gained loops are indicated by blue, purple and red arrows respectively. Results of individual replicates are shown. **c,** Boxplots showing the log_2FC in loop strength upon STAG2 depletion across indicated loop-size bins, comparing loops identified by the optimized HICCUPS-based pipeline and by cooltools dots in *Stag2*^{mAID} cells. Results from replicate-merged data and individual biological replicates are shown. Both loop-calling approaches reveal a consistent trend, showing enhanced large-loop formation in late-G1 upon STAG2 depletion. The number of loops analyzed for each loop-calling method, dataset and loop-size bin is provided in the Source Data file. *P* values were calculated using two-sided paired Wilcoxon tests. Hi-C analyses in this figure include results from replicate-merged Hi-C data as well as individual Hi-C biological replicates. For all box plots, central lines denote medians; box limits denote the 25th-75th percentiles; whiskers denote the 5th-95th percentiles. Source data are provided as a Source Data file.

Supplementary Figure 6



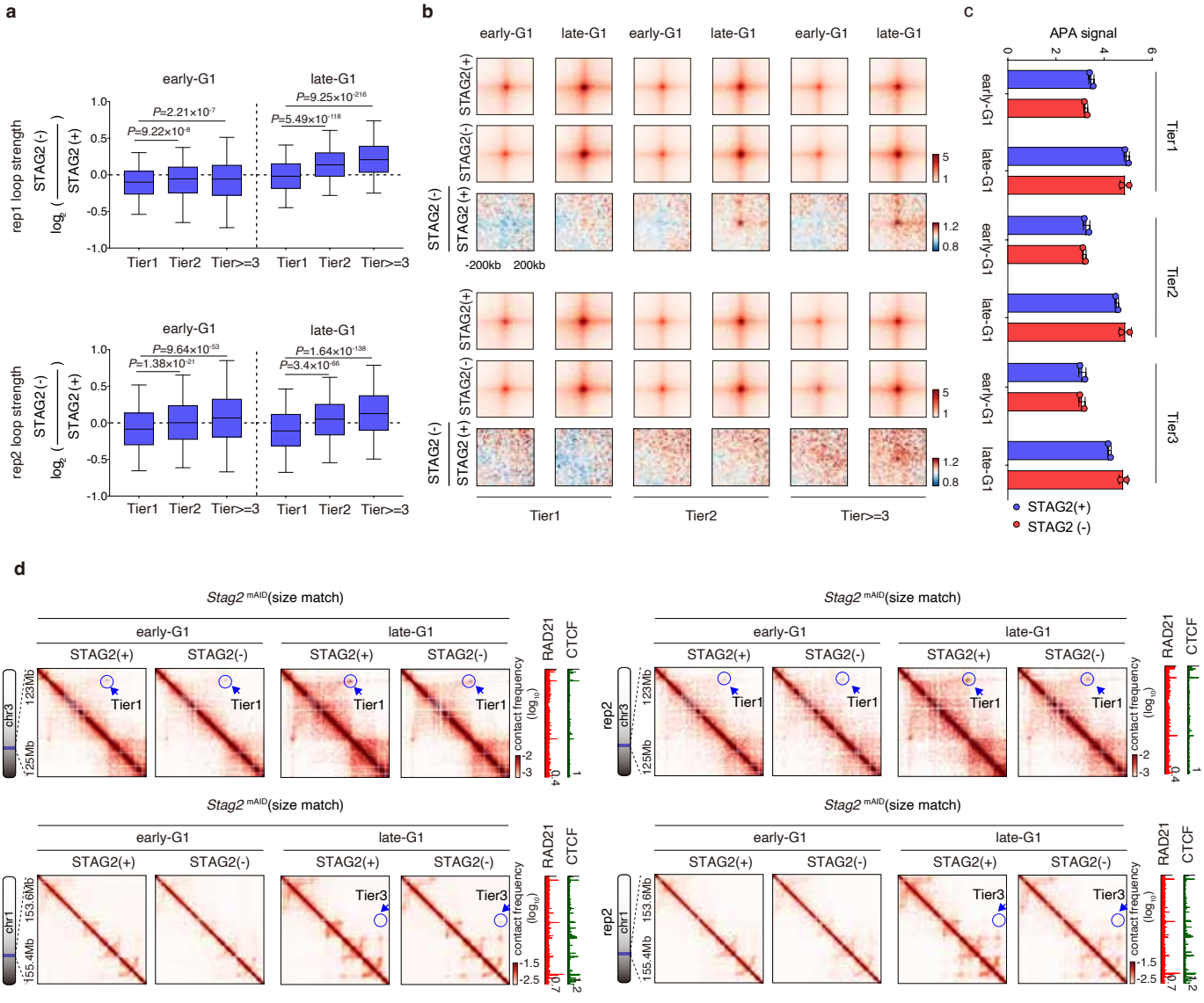
Supplementary Fig. 6: STAG2 depletion does not alter STAG1 and RAD21 chromatin occupancy. a, Heat maps of STAG1 ChIP-seq signals detected with anti-STAG1 antibody (abcam, #ab4455) in asynchronous *Stag2*^{mAID} cells with or without 5-Ph-IAA treatment. Results from replicate-merged samples and three independent biological replicates are shown. Both SCF- and CPM-normalized signals indicate that STAG2 depletion does not detectably alter STAG1 chromatin occupancy. **b** Same as (a), using a second anti-STAG1 antibody (abcam, #ab317301). Results from replicate-merged samples and two independent biological replicates are shown. **c**, Same as (a), but for RAD21 ChIP-seq in asynchronous *Stag2*^{mAID} cells. **d**, Representative genome browser tracks corresponding to (c), showing no obvious change in RAD21 occupancy at the indicated locus. **e**, Same as (b), but for late-G1 *Stag2*^{mAID} cells, showing no detectable increase in STAG1 chromatin occupancy upon STAG2 depletion. **f**, Representative genome browser tracks corresponding to (e). **g**, Representative immunoblots from chromatin fractionation experiments in *Stag2*^{mAID} cells showing that STAG2 is efficiently depleted from the chromatin fraction upon 5-Ph-IAA treatment, whereas chromatin-associated STAG1, SMC1, and RAD21 remain largely unchanged (cytoplasmic, cytoplasmic fraction; soluble nuclear, soluble nuclear fraction; chr, chromatin fraction). **h**, Quantification of (g), Signals were normalized to H3 and expressed relative to parental G1E-ER4 cells, which were set to 1. STAG2 was efficiently depleted from the chromatin fraction upon 5-Ph-IAA treatment, whereas chromatin-associated STAG1, SMC1, and RAD21 remained largely unchanged. Bars indicate mean and error bars indicate s.e.m. $n = 3$. P values were calculated using two-sided Student's t-tests. Source data are provided as a Source Data file.

Supplementary Figure 7



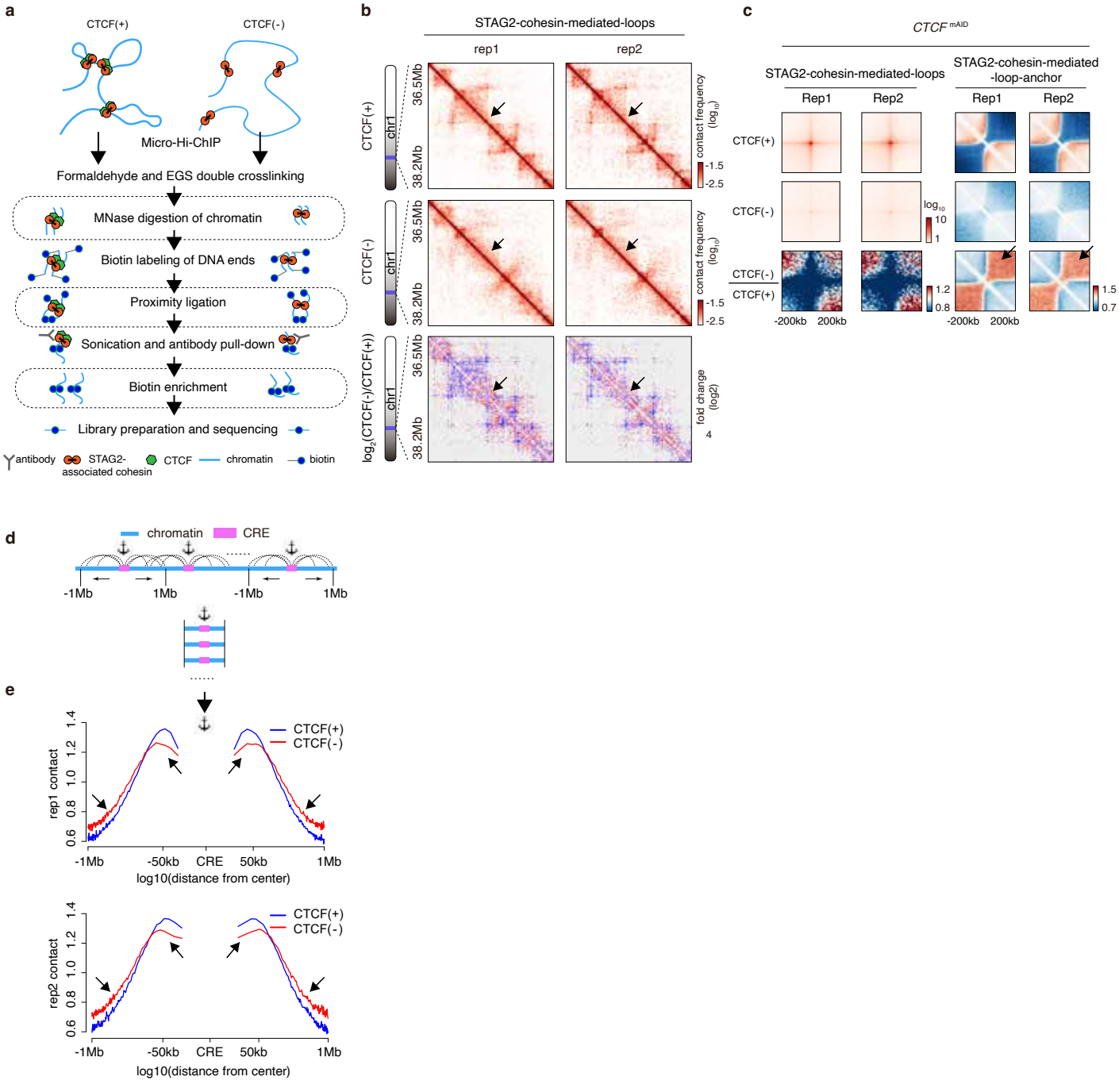
Supplementary Fig. 7: STAG1-associated loops are larger than STAG2-associated loops in G1E-ER4 cells. a, Schematic illustration of the Micro-HiChIP workflow performed in G1E-ER4 cells using STAG1 or STAG2 antibodies. **b,** Venn diagrams showing overlap analysis of loops identified by STAG1 and STAG2 Micro-HiChIP in two biological replicates. **c,** Representative contact maps from two biological replicates showing STAG1- and STAG2-associated loops in G1E-ER4 cells. Blue arrows indicate representative STAG1-associated loops, which are generally larger than STAG2-associated loops. **d,** Density plots showing the distribution of loop sizes for STAG1- and STAG2-associated loops in two biological replicates. In replicate 1, n=38,390 STAG1-associated loops and 24,960 STAG2-associated loops; in replicate 2, n=15,812 STAG1-associated loops and 10,922 STAG2-associated loops. *P* values were calculated using two-sided Wilcoxon rank-sum tests. **e,** Boxplots showing loop-size distributions of STAG1-only loops, loops shared by STAG1 and STAG2, and STAG2-only loops in two biological replicates. In replicate 1, n=17,963 STAG1-only loops, 20,427 shared loops and 4,533 STAG2-only loops; in replicate 2, n=7,437 STAG1-only loops, 8,375 shared loops and 2,547 STAG2-only loops. STAG1-only loops are the largest, shared loops show intermediate sizes, and STAG2-only loops are the smallest. *P* values were calculated using two-sided Wilcoxon rank-sum tests. For all box plots, central lines denote medians; box limits denote the 25th-75th percentiles; whiskers denote the 5th-95th percentiles. Source data are provided as a Source Data file.

Supplementary Figure 8



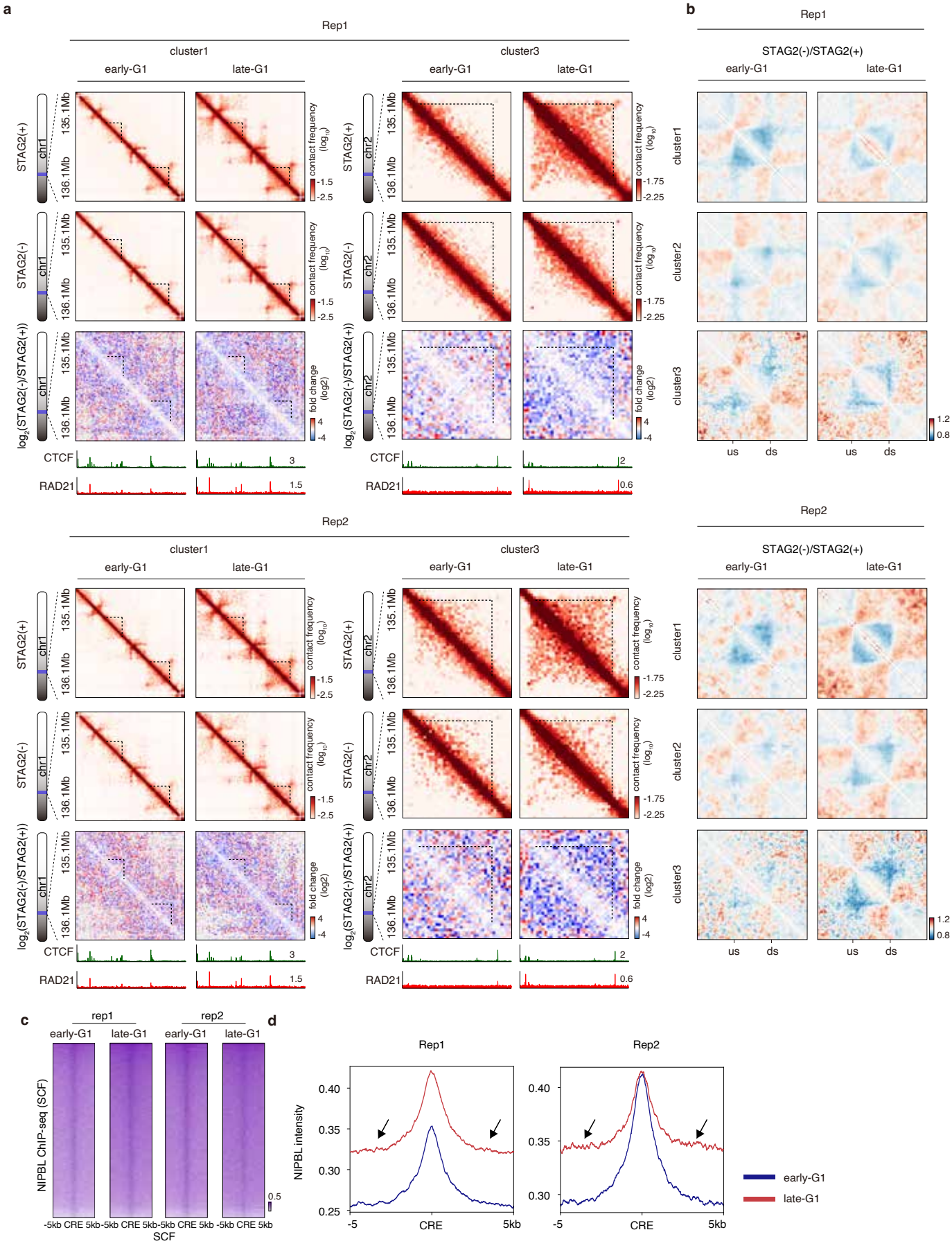
Supplementary Fig. 8: Impacts of Stag2 loss on structural loops of different hierarchical tiers. a, Boxplots showing the impacts of STAG2 loss on loops across different tiers. Log_2FC values are calculated for each biological replicate respectively. The numbers of loops analyzed for Tier1, Tier2 and Tier≥3 were 3,530, 2,594 and 2,860 in early-G1 rep1; 3,534, 2,598 and 2,866 in early-G1 rep2; 3,526, 2,596 and 2,854 in late-G1 rep1; and 3,530, 2,597 and 2,855 in late-G1 rep2, respectively. *P* values are calculated using a two-sided Wilcoxon rank-sum test. **b**, APA plots showing the changes in structural loops across different tiers upon STAG2 loss in early- and late-G1 phase. Data for two biological replicates are shown independently. **c**, Bar graphs showing the quantification of APA plots in (**b**). **d**, KR-balanced Hi-C contact maps showing representative size-matched Tier1 and Tier3 structural loops in early- and late-G1 phase cells with or without STAG2. Maps for individual biological replicates are shown. Late-G1 RAD21 and CTCF ChIP-seq tracks are shown on the right. For all box plots, central lines denote medians; box limits denote the 25th-75th percentiles; whiskers denote the 5th-95th percentiles. Source data are provided as a Source Data file.

Supplementary Figure 9



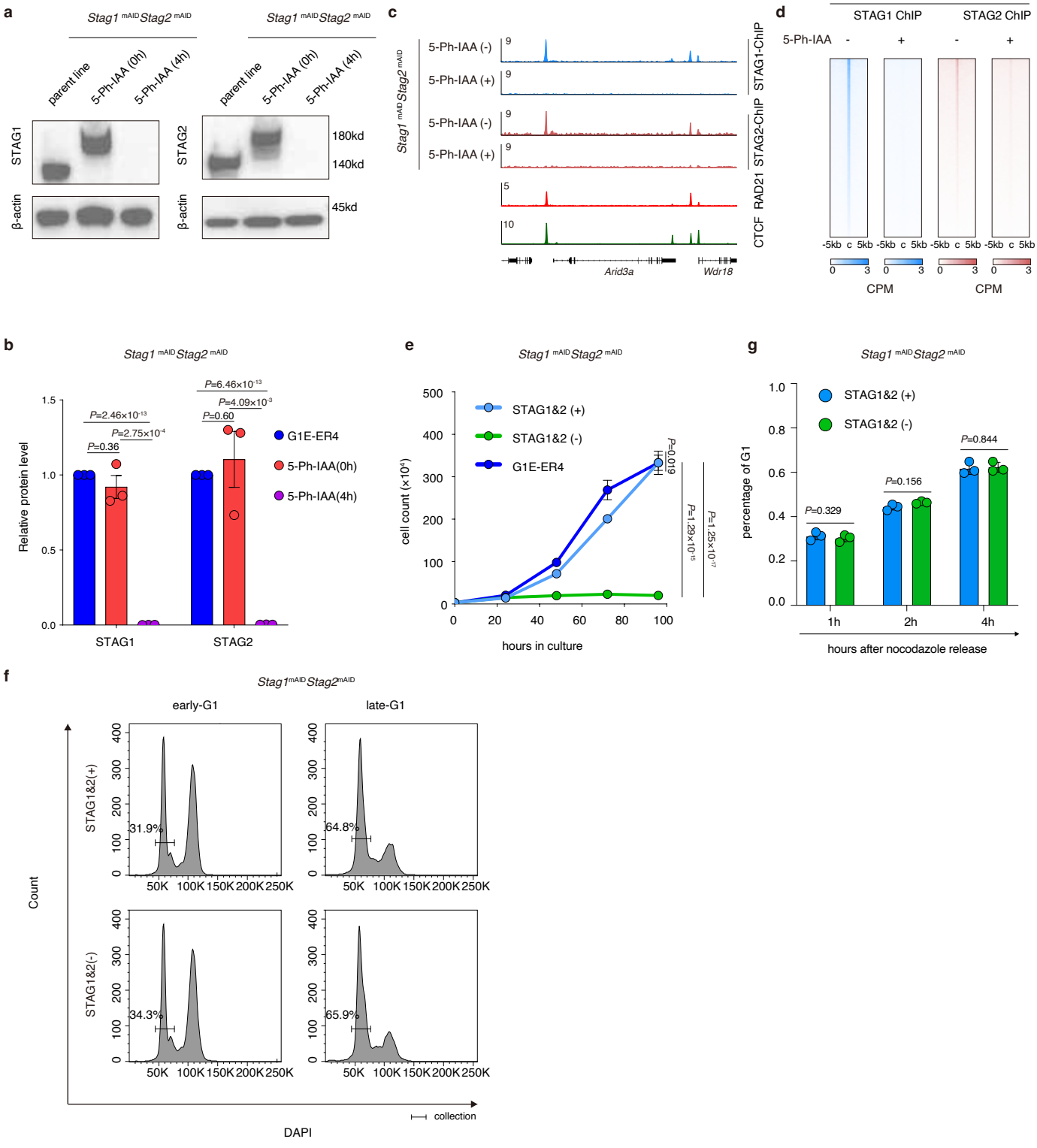
Supplementary Fig. 9: CTCF depletion enables STAG2-associated cohesin to bypass loop anchors and form more distal contacts. a, Schematic illustration of the Micro-HiChIP workflow used to profile STAG2-associated chromatin interactions in *Ctcf*^{mAID} cells before and after CTCF depletion. **b,** Representative STAG2 Micro-HiChIP contact maps showing STAG2-cohesin-mediated loops in the presence or absence of CTCF. Data from two biological replicates are shown. Differential maps of $\log_2$[CTCF(-)/CTCF(+)] are shown below, highlighting increased distal contacts across former loop-anchor regions upon CTCF loss. **c,** APA plots showing STAG2-cohesin-mediated loops in *Ctcf* ^{mAID} cells with or without CTCF, together with corresponding ratio maps, for two biological replicates. Right, APA and ratio plots centered on STAG2-cohesin-mediated loop anchors. Upon CTCF depletion, STAG2-associated cohesin shows increased contact formation across loop anchors, consistent with weakened insulation and enhanced long-range interactions. **d,** Schematic illustration of the analysis shown in (e). For all CREs, chromatin contacts between each CRE and regions within ±1 Mb were quantified to examine how CTCF depletion alters contact profiles around CRE-centered loci. **e,** Compiled virtual 4C plots centered around CREs in two biological replicates, showing contact profiles as a function of $\log_{10}$(distance from the CRE center). Upon CTCF depletion, contact frequency is reduced at regions proximal to CREs but increased at more distal regions. Arrows indicate these reciprocal changes, showing that interactions emanating from CREs extend to longer genomic distances in the absence of CTCF. Source data are provided as a Source Data file.

Supplementary Figure 10



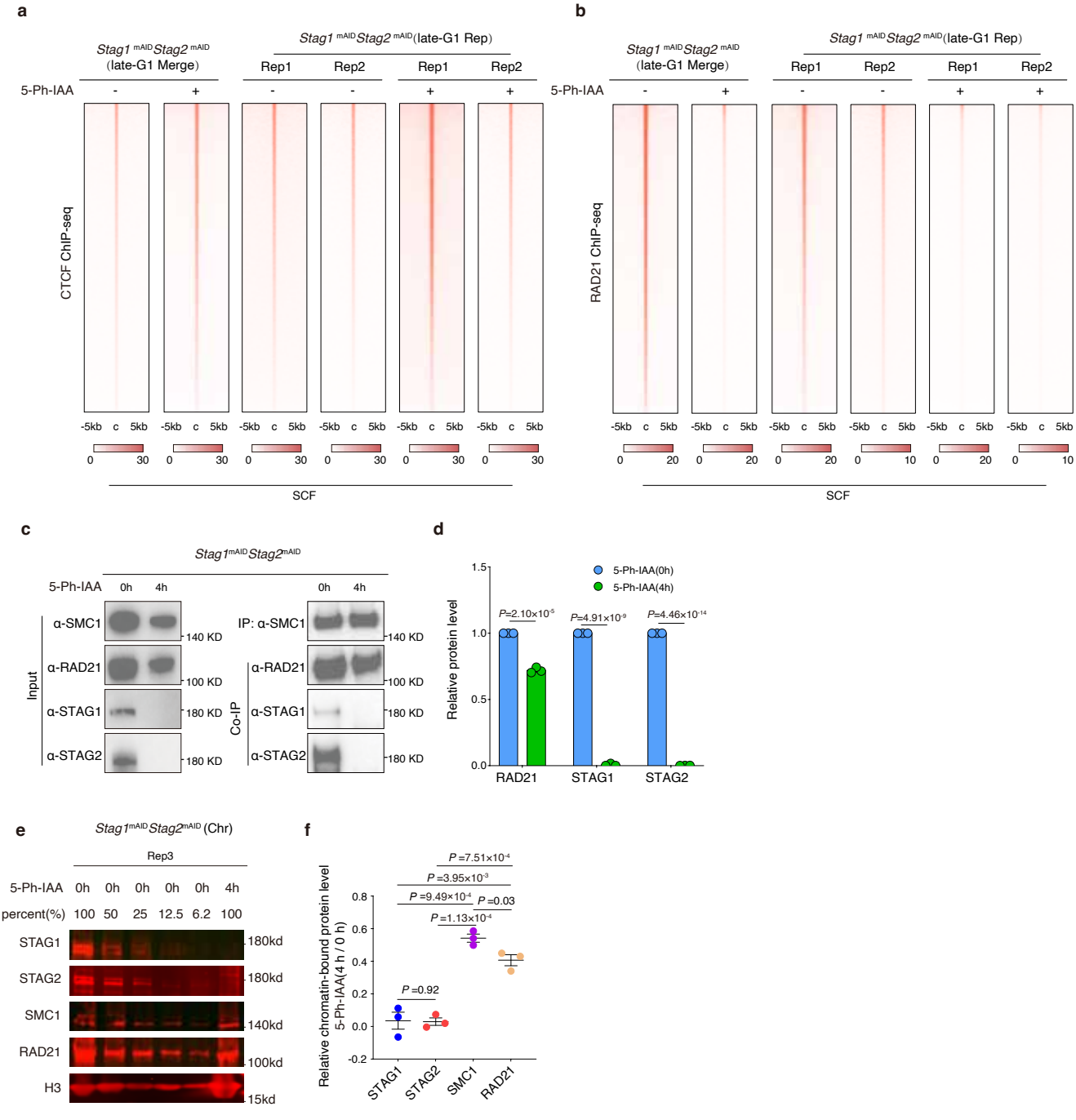
Supplementary Fig. 10: Additional data supporting chromatin context-dependent regulation of loop extrusion by STAG2. a, KR-balanced Hi-C contact maps showing the changes in cluster 1 (left) and cluster 3 (right) loops upon STAG2 depletion in early- and late-G1 phase. Dotted boxes demarcate intra-loop contacts. Data from individual biological replicates are shown. Corresponding CTCF and RAD21 ChIP-seq tracks are shown below. **b,** Compiled and rescaled contact maps showing the distinct impact of STAG2 loss on intra-loop contacts across all three clusters. "us" and "ds" denote the upstream and downstream loop anchors, respectively. Data from individual biological replicates are shown. **c,** Heat maps of SCF-normalized NIPBL ChIP-seq signals centered at CREs (±5 kb) in early-G1 and late-G1 G1E-ER4 cells. Data from two biological replicates are shown. **d,** Metaplots showing NIPBL ChIP-seq signal centered at CREs (±5 kb) in early-G1 and late-G1 G1E-ER4 cells. In both biological replicates, NIPBL enrichment around CREs is stronger in late-G1 than in early-G1. Source data are provided as a Source Data file.

Supplementary Figure 11



Supplementary Fig. 11: Characterization of the *Stag1*^{mAID}*Stag2*^{mAID} cell line. a, Immunoblot analysis of endogenous STAG1 and STAG2 protein levels in the parental G1E-ER4 cells and *Stag1*^{mAID}*Stag2*^{mAID} cells treated with 5-Ph-IAA for the indicated durations. STAG1 and STAG2 were both efficiently depleted after 4 h of 5-Ph-IAA treatment. Three independent biological replicates were performed. **b,** Quantification of (**a**), showing complete depletion of both STAG1 and STAG2 after 4 h of 5-Ph-IAA treatment. Signals were normalized to β-actin and expressed relative to parental G1E-ER4, which was set to 1. Bars indicate mean and error bars indicate s.e.m.; $n = 3$. *P* values were calculated using two-sided Student's *t*-tests. **c,** Representative genome browser tracks showing loss of STAG1 and STAG2 ChIP-seq signals upon 5-Ph-IAA treatment in *Stag1*^{mAID}*Stag2*^{mAID} cells. RAD21 and CTCF ChIP-seq tracks for the same region are shown below. **d,** Heat maps of CPM-normalized STAG1 and STAG2 ChIP-seq signals centered at peak summits (±5 kb) in *Stag1*^{mAID}*Stag2*^{mAID} cells with or without 5-Ph-IAA treatment, showing efficient removal of chromatin-bound STAG1 and STAG2 after 5-Ph-IAA treatment. **e,** Growth curves of *Stag1*^{mAID}*Stag2*^{mAID} cells with or without STAG1 and STAG2 co-depletion, shown together with the unedited parental G1E-ER4 cells. Data are mean ± s.d. from three independent biological replicates. *P* values were calculated using two-way repeated-measures ANOVA with Tukey's multiple-comparisons test. **f,** Representative flow-cytometry profiles of DNA content after nocodazole release, showing the early-G1 and late-G1 populations of *Stag1*^{mAID}*Stag2*^{mAID} cells with or without STAG1 and STAG2 depletion. **g,** Bar graphs (mean ± s.d.; n = 3 biological replicates) showing the percentage of G1-phase cells at the indicated time points after nocodazole release in *Stag1*^{mAID}*Stag2*^{mAID} cells with or without 5-Ph-IAA treatment. These results indicate that short-term cell-cycle progression after mitotic release is not detectably altered by co-depletion of STAG1 and STAG2. *P* values were calculated using two-tailed Student's *t*-tests. Source data are provided as a Source Data file.

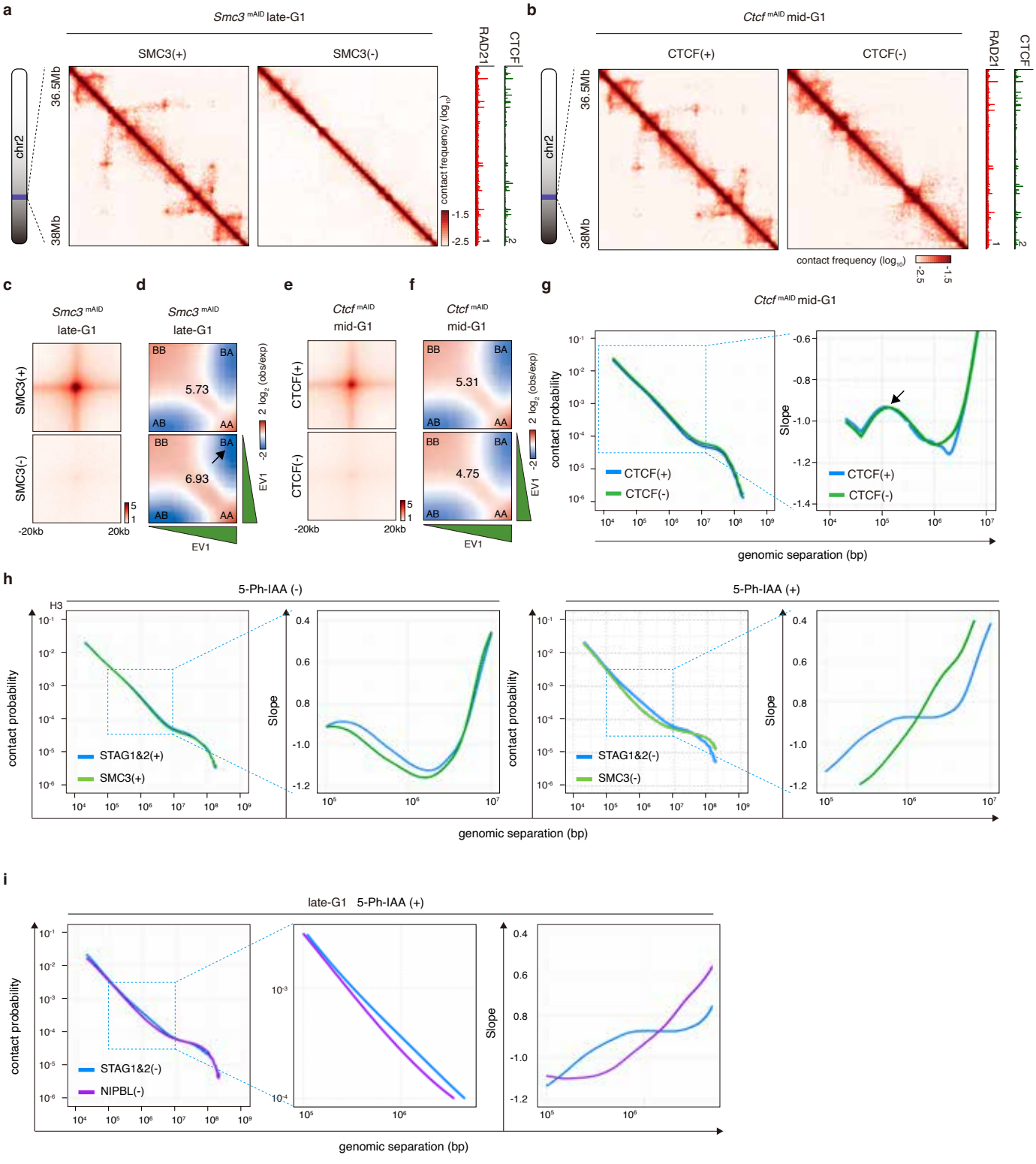
Supplementary Figure 12



Supplementary Fig. 12: Residual cohesin persists after STAG1 and STAG2 co-depletion. a, Heat maps of SCF-normalized CTCF ChIP-seq signals centered at peak summits (±5 kb) in late-G1 *Stag1*^{mAID}*Stag2*^{mAID} cells with or without 5-Ph-IAA treatment. Data from replicate-merged samples and two individual biological replicates are shown. CTCF chromatin occupancy is largely unchanged upon STAG1 and STAG2 co-depletion. **b,** Heat maps of SCF-normalized RAD21 ChIP-seq signals centered at peak summits (±5 kb) in late-G1 *Stag1*^{mAID}*Stag2*^{mAID} cells with or without 5-Ph-IAA treatment. Data from replicate-merged samples and two individual biological replicates are shown. RAD21 chromatin occupancy is markedly reduced upon STAG1 and STAG2 co-depletion. **c,** Co-immunoprecipitation using anti-SMC1 in *Stag1*^{mAID}*Stag2*^{mAID} cells before and after 4 h 5-Ph-IAA treatment. After STAG1 and STAG2 co-depletion, neither STAG1 nor STAG2 was detectably co-immunoprecipitated with SMC1, indicating efficient removal of both STAG proteins from cohesin complexes. In contrast, RAD21 remained associated with SMC1, indicating that cohesin complexes persist after STAG1 and STAG2 loss. Three independent biological replicates were performed. **d,** Quantification of SMC1 co-immunoprecipitation in (**c**). Co-immunoprecipitated RAD21, STAG1, and STAG2 signals were normalized to the corresponding immunoprecipitated SMC1 signal, and the 0 h sample was set to 1 for each protein. STAG1 and STAG2 association with SMC1 was nearly abolished after 4 h of 5-Ph-IAA treatment. Bars indicate mean and error bars indicate s.e.m; dots represent independent experiments; $n = 3$. P values were calculated using two-sided Student's t-tests. **e**, Representative fluorescence immunoblots of chromatin fractions from *Stag1*^{mAID}*Stag2*^{mAID} cells. Undepleted 0 h chromatin samples were serially diluted twofold, as indicated, and loaded alongside chromatin fractions collected after 4 h of 5-Ph-IAA treatment. STAG1, STAG2, SMC1 and RAD21 were detected, with H3 used as a chromatin loading control. **f**, Quantification of residual chromatin-bound protein levels after 4 h of 5-Ph-IAA treatment. Band intensities were normalized to H3 and then expressed relative to the

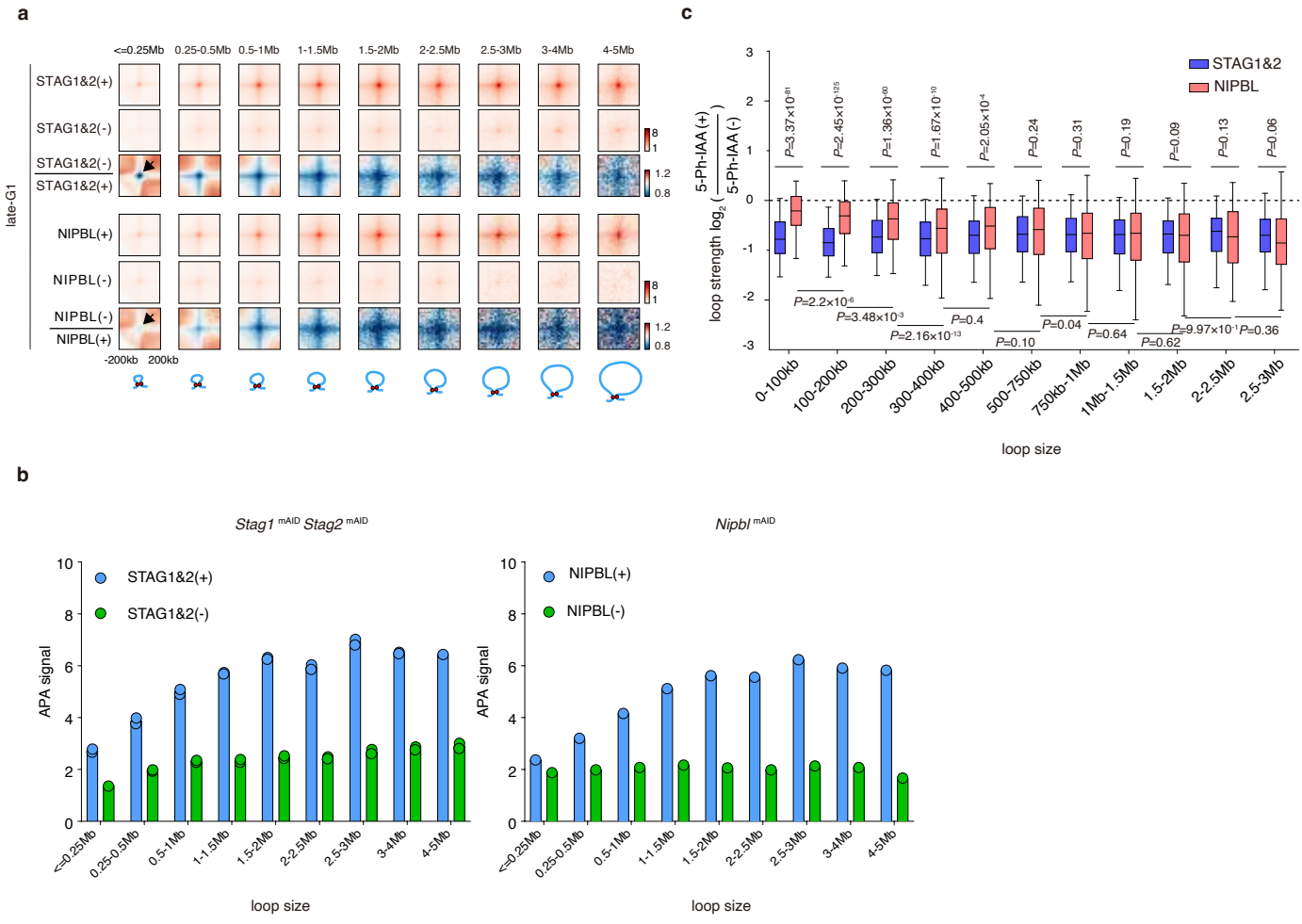
corresponding undepleted 0 h control. Each dot represents one biological replicate; n = 3. P values were calculated using two-tailed Student's t-test. Source data are provided as a Source Data file.

Supplementary Figure 13



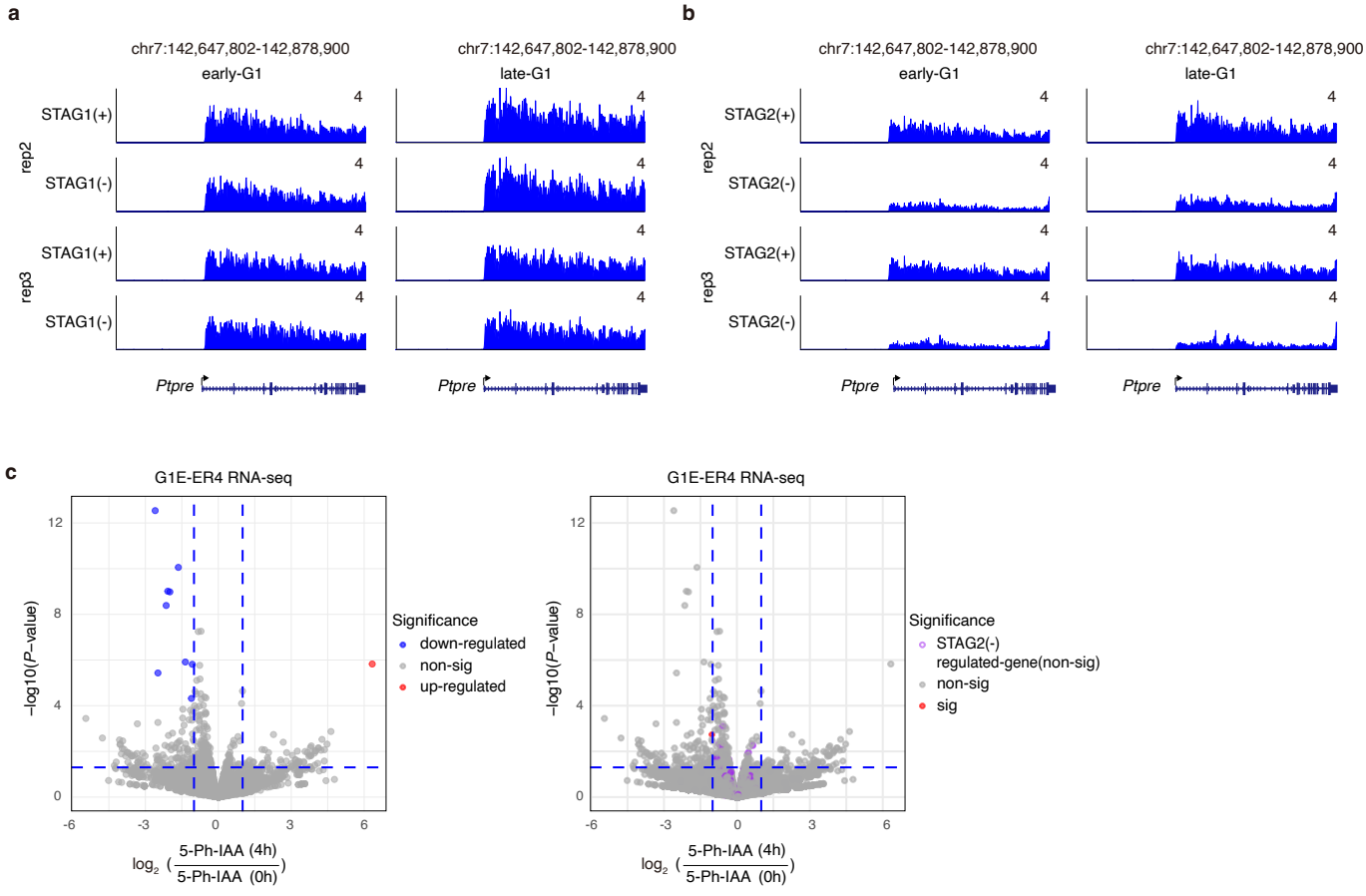
Supplementary Fig. 13: Cohesin retains loop extrusion capacity upon STAG1 and STAG2 co-depletion. a, KR-balanced Hi-C contact maps of late-G1 *Smc3*^{mAID} cells with or without SMC3 depletion, showing complete loss of structural loops upon SMC3 depletion. RAD21 and CTCF ChIP-seq tracks are shown on the right. **b,** KR-balanced Hi-C contact maps of mid-G1 *CTCF*^{mAID} cells with or without CTCF depletion, showing loss of structural loops upon CTCF depletion. RAD21 and CTCF ChIP-seq tracks are shown on the right. **c,** APA plots showing complete loss of structural loops in late-G1 upon SMC3 depletion. **d,** Saddle plots showing strengthened chromatin compartmentalization upon SMC3 depletion in late-G1. **e,** APA plots showing loss of structural loops in mid-G1 upon CTCF depletion. **f,** Saddle plots showing modestly reduced chromatin compartmentalization upon CTCF depletion in mid-G1. **g,** P_S curves and corresponding slope analysis for mid-G1 *Ctcf*^{mAID} cells with or without CTCF depletion, showing limited effects of CTCF loss on short-range contact scaling. **h,** P_S curves and corresponding slope analysis comparing *Smc3*^{mAID} and *Stag1*^{mAID}*Stag2*^{mAID} samples under the indicated 5-Ph-IAA conditions. Compared with SMC3 depletion, STAG1 and STAG2 co-depletion causes a milder reduction in short-range contacts, consistent with residual loop extrusion activity. **i,** P_S curves and corresponding slope analysis comparing late-G1 *Stag1*^{mAID}*Stag2*^{mAID} cells with NIPBL-depleted cells under 5-Ph-IAA treatment. Compared with NIPBL depletion, STAG1 and STAG2 co-depletion retains higher short-range contact frequencies, further supporting the persistence of residual loop extrusion after STAG1 and STAG2 loss. Source data are provided as a Source Data file.

Supplementary Figure 14



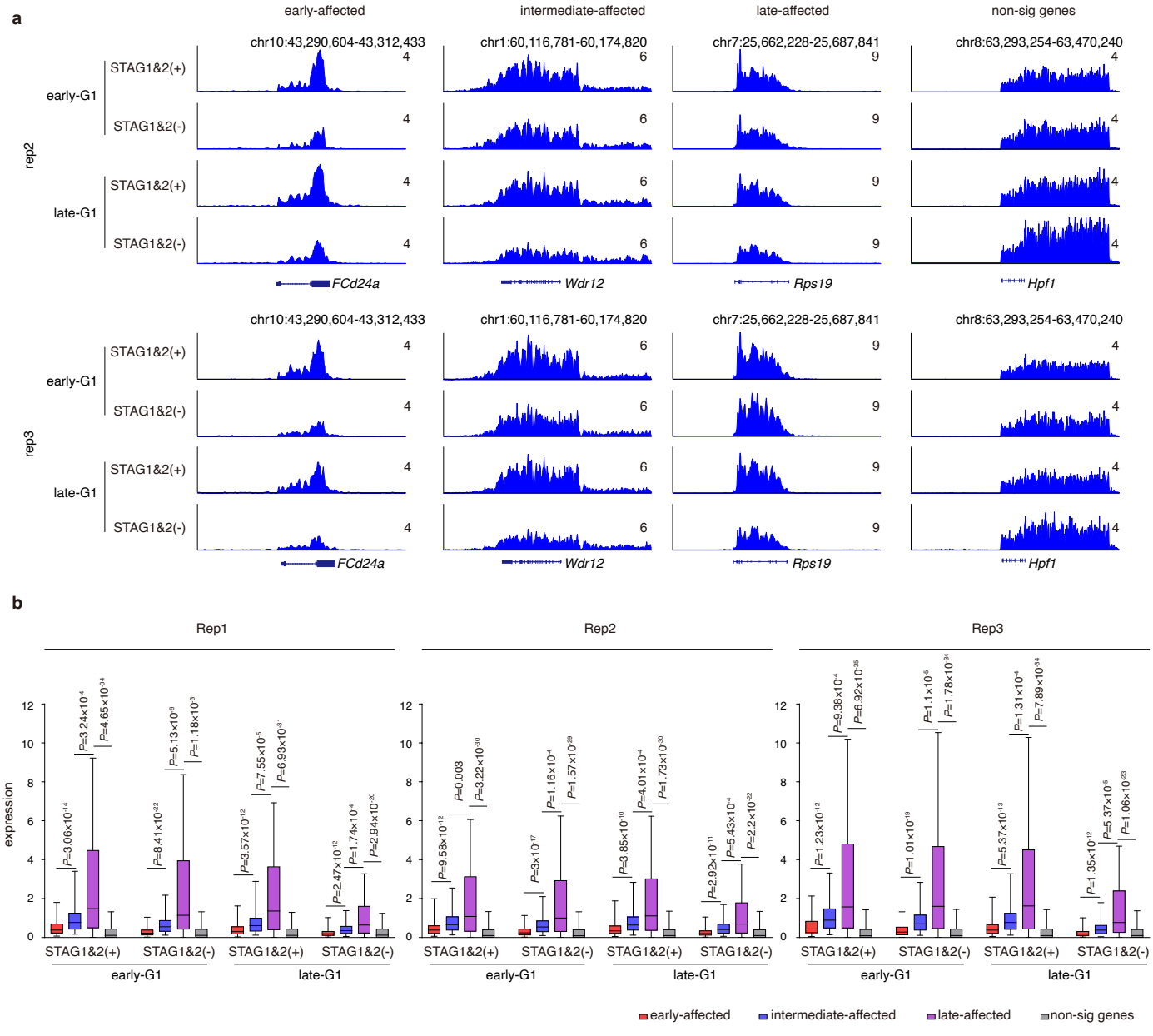
Supplementary Fig. 14: STAG1 and STAG2 co-depletion does not affect the extruding processivity of chromatin-associated cohesin. a, APA plots, showing that STAG1 and STAG2 co-depletion reduces structural loops uniformly, regardless of their size (black arrow, upper panel). In contrast, NIPBL depletion, which affects cohesin extrusion capacity, causes a size-dependent loss of loops, with smaller loops being less affected (black arrow, lower panel). **b**, Bar plots showing the quantification of APA plots in (**a**). For STAG1 and STAG2 co-depletion, each dot represents a biological replicate (n=2). For NIPBL depletion, data are shown for the replicate-merged samples. **c**, Boxplots showing the $\log_2$FC in structural loop strength, revealing the distinct effects of STAG1 and STAG2 co-depletion versus NIPBL depletion on loops of various sizes. Comparisons between STAG1 and STAG2 co-depletion and NIPBL depletion within the same loop-size bin used two-sided paired Wilcoxon signed-rank tests, whereas comparisons between adjacent loop-size bins within NIPBL-depleted cells used two-sided Wilcoxon rank-sum tests. The numbers of structural loops analyzed for each condition and loop-size bin are provided in the Source Data file. All Hi-C analyses in this figure were performed using replicate-merged Hi-C data from two biological replicates. For all box plots, central lines denote medians; box limits denote the 25th-75th percentiles; whiskers denote the 5th-95th percentiles. Source data are provided as a Source Data file.

Supplementary Figure 15



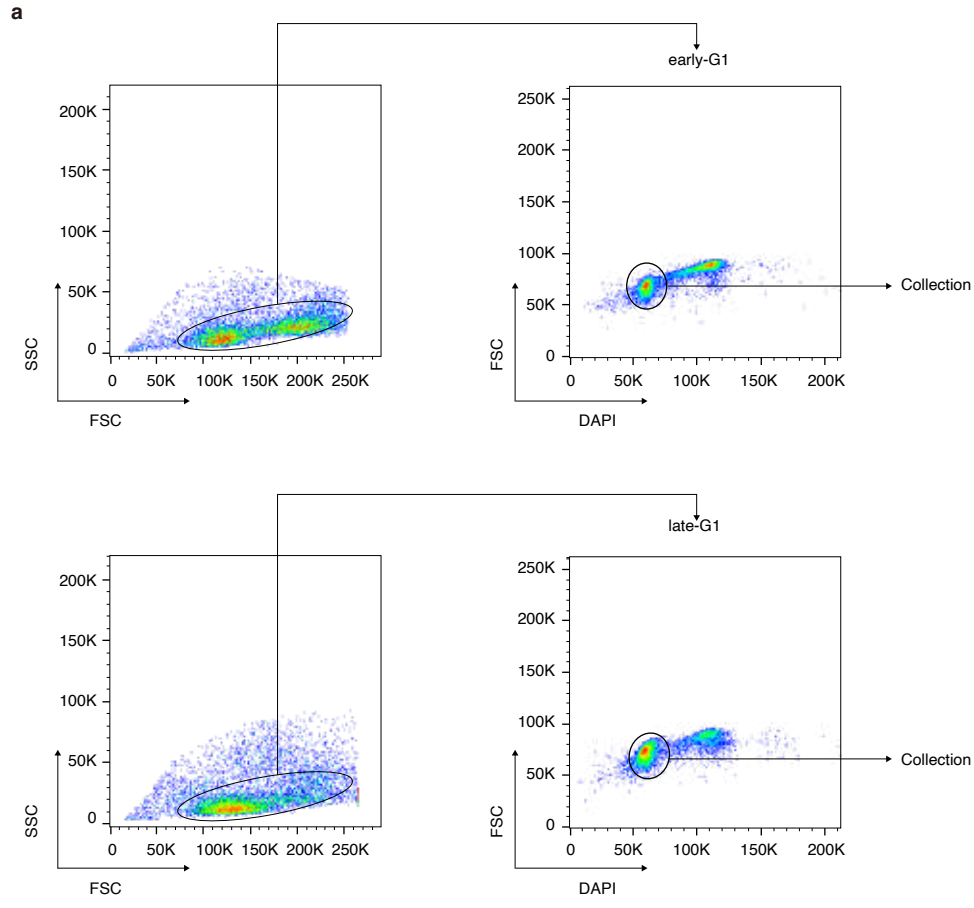
Supplementary Fig. 15: Additional validation of STAG1 and STAG2 dependent transcriptional changes. a, Genome browser tracks showing TT-seq signals at the *Ptpre* locus in additional biological replicates of early-G1 and late-G1 cells with or without STAG1 depletion. **b,** Similar to (a), genome browser tracks showing TT-seq signals at the *Ptpre* locus in additional biological replicates of early-G1 and late-G1 cells with or without STAG2 depletion. **c,** RNA-seq analysis of parental G1E-ER4 cells treated with 5-Ph-IAA for 4 h, performed in three biological replicates, showing that auxin treatment alone alters the expression of only a small number of genes (left). Genes whose nascent transcription is affected by STAG2 depletion are highlighted on the same RNA-seq background (right) and are largely not significantly changed by 5-Ph-IAA treatment in parental cells, indicating that the transcriptional changes observed upon STAG2 depletion are not attributable to auxin treatment itself. Source data are provided as a Source Data file.

Supplementary Figure 16



Supplementary Fig. 16: Additional biological replicates validate transcriptional changes upon STAG1 and STAG2 co-depletion. a, Genome browser tracks showing TT-seq signals from additional biological replicates in early-G1 and late-G1 cells with or without STAG1 and STAG2 co-depletion. Tracks for four representative loci are shown: *Fcd24a* (early-affected), *Wdr12* (intermediate-affected), *Rps19* (late-affected), and *Hpf1* (non-significant). **b,** Boxplots showing TT-seq signals across gene bodies for the early-affected, intermediate-affected, late-affected, and non-significant gene groups. Data are shown for early-G1 and late-G1 cells with or without STAG1 and STAG2 co-depletion. Results from three independent biological replicates are shown. For each biological replicate and condition, n=223 early-affected genes, 213 intermediate-affected genes, 112 late-affected genes and 17,141 non-significant and undetectably expressed genes. *P* values were calculated using two-sided Wilcoxon rank-sum tests. For all box plots, central lines denote medians; box limits denote the 25th-75th percentiles; whiskers denote the 5th-95th percentiles. Source data are provided as a Source Data file.

Supplementary Figure 17



Supplementary Fig. 17: Flow-cytometry gating strategy for isolation of early- and late-G1 cells. a, Representative sequential gating strategy used for FACS sorting of early-G1 and late-G1 cells throughout this study. Cells were first gated based on FSC and SSC to exclude debris and abnormal events. The gated population was then plotted by DAPI intensity and FSC, and early-G1 or late-G1 populations were isolated according to DNA-content profiles after release from mitotic arrest. The upper panels show the gating strategy for early-G1 sorting, and the lower panels show the gating strategy for late-G1 sorting. This gating strategy applies to all early-G1 and late-G1 FACS-sorted samples used for Hi-C and ChIP-seq analyses in the main and supplementary figures.